Applied Catalysis B: Environmental 162 (2015) 167–173

Contents lists available at ScienceDirect

Applied Catalysis B: Environmental

journal homepage: www.elsevier.com/locate/apcatb

In situ generated TiO_2 over zeolitic supports as reusable photocatalysts for the degradation of dichlorvos

Silvina Gomez[a,c,*], Candelaria Leal Marchena[a,c], María S. Renzini[a,c], Luis Pizzio[b,c], Liliana Pierella[a,c]

[a] CITeQ (Centro de Investigación y Tecnología Química), Facultad Regional Córdoba, Universidad Tecnológica Nacional, Maestro López esq. Cruz Roja Argentina, Córdoba, Argentina
[b] Centro de Investigación y Desarrollo en Ciencias Aplicadas "Dr. J. J. Ronco" (CINDECA), Departamento de Química, Facultad de Ciencias Exactas, UNLP-CCT La Plata, 47 Nº 257, 1900 La Plata, Buenos Aires, Argentina
[c] CONICET, Argentina

ARTICLE INFO

Article history:
Received 27 January 2014
Received in revised form 2 June 2014
Accepted 27 June 2014
Available online 5 July 2014

Keywords:
Photodegradation
Dichlorvos
Zeolites
Titanium dioxide
Reusable catalyst

ABSTRACT

Materials based on titania supported on zeolitic matrices (HBETA, HY and HZSM5) were synthesized by in situ generation of TiO_2. The supported catalysts characterized by XRD indicate the presence of the anatase phase alone. The materials were also characterized by FTIR, S_{BET}, and UV-VIS DRS. A high TiO_2 content produced lower degradation, due to the presence of TiO_2 particle aggregates of greater size on the zeolite matrix surface, as evidenced by the calculated crystal size. TiO_2/HBETA(20%) presented more activity than TiO_2 supported on the other matrices due to higher adsorption of dichlorvos on HBETA. It has more surface area and a lower band gap value too, which makes it more effective. The mineralization degree is lower than the degradation percentage due to the formation of organophosphorous intermediates that are less toxic than the starting material. The complete degradation and mineralization of the pollutant was obtained in 360 and 540 min of reaction with TiO_2/HBETA(20%), respectively. This catalyst resulted in degradation percentages close to that of commercial TiO_2 P25. The main advantage of supported catalysts is their easy separation and reuse, in this case resulting in a very low activity loss during eight cycles. These materials present suitable properties to be used as catalysts in the photocatalytic treatment of wastewater that contains pesticide dichlorvos in water.

1. Introduction

The increasing demand and shortage of clean water sources due to the rapid development of industrialization, population growth and long-term droughts have become an issue worldwide. With this growing demand, various practical strategies and solutions have been adopted to yield more viable water resources [1].

In recent years, an alternative to conventional methods for the decontamination of water has been provided, which is known as "Advanced Oxidation Processes" (AOPs) and is based on the generation of very reactive species such as hydroxyl radicals that quickly and nonselectively oxidize a broad range of organic pollutants [2]. One of these AOPs that has attracted special attention is heterogeneous photocatalysis, employing UV–Vis light as energy source and a solid catalyst as active site for water detoxification. Indeed, the subject has become an area of intensive research. The main advantage of photocatalysis over conventional water treatment methods is that a wide range of organic compounds can be completely mineralized, leading to the formation of carbon dioxide, water, and inorganic mineral salts [3]. The generated $OH^{\bullet}$ radicals interact with organic pollutants, leading to progressive degradation that is followed by complete mineralization. Among these heterogeneous photocatalysts, TiO_2 has been considered as a promising one for the remediation of wastewater treatment [4–7]. TiO_2 is presented as one of the most appropriate semiconductor materials to be employed as a photocatalyst due to its high activity in the photodegradation of organic compounds, low cost, low toxicity, and chemical stability [8].

The main drawbacks of TiO_2 catalysts are the need for complex filtration procedures and the high turbidity that decreases the radiation flux. The practical applications of TiO_2 are limited because

* Corresponding author at: CITeQ (Centro de Investigación y Tecnología Química), Facultad Regional Córdoba, Universidad Tecnológica Nacional, Maestro López esq. Cruz Roja Argentina, Córdoba, Argentina. Tel.: +54 351 469 0585; fax: +54 351 469 0585.
E-mail address: sgomez@scdt.frc.utn.edu.ar (S. Gomez).

http://dx.doi.org/10.1016/j.apcatb.2014.06.047
0926-3373/

of the problems of low recovery efficiency of TiO_2 fine particles, fast recombination rate of the photogenerated electron–hole pair, and a low quantum yield in the photocatalytic reactions in aqueous solutions [9].

Such problems have motivated the development of supported photocatalysts in which TiO_2 is immobilized on different adsorbent materials. Immobilizing TiO_2 on substrates such as a glass matrix, optical fiber and stainless steel plate eliminates the problem of agglomeration, although the photocatalytic efficiency of immobilized TiO_2 is less than that of the suspended TiO_2 particles [10]. Besides, the specific surface area also decreases due to the fixing of TiO_2 on nonporous supports, which reduces the adsorption capacity. For photocatalytic decomposition of a target compound, its adsorption on the TiO_2 surface is essential prior to the surface reaction. Furthermore, organic pollutants generally occur in low concentrations (ppm level or below) and pre-concentration of the substrates on the surface where photons are absorbed is a desirable feature for effective photodegradation [11].

The supports should withstand reactive oxidative radical attack during illumination, have long-term stability, prevent TiO_2 leaching during light irradiation, and have the ability to delocalize electrons. Many reported studies deal with the immobilization of TiO_2 over different inert porous supports [10,12–23]. In this context, zeolites have attracted greater attention due to their adsorption capacity, which helps in pooling the pollutants to the vicinity of the TiO_2 surface and also leads to faster degradation [7,23,24].

Zeolites are microporous crystalline aluminosilicates with structural features, such as the ability to trigger photoinduced electron donor and acceptor reactions, which make them attractive hosts for photochemical applications [25,26]. Furthermore, zeolites delocalize band-gap excited electrons of TiO_2 and minimize electron–hole recombination. Due to these interesting properties, zeolites are attractive catalyst supports in the treatment of pesticide-contaminated water. TiO_2 supported on zeolites, which have large surface area and light transparent nature, increases the adsorption capacity, and the uniform diffusion of pesticide pollutants leads to efficient degradation [27].

Increasing pesticide application and improper wastewater disposal methods contaminate water resources and severely affect the ecology as well as the environment [24]. Insecticides are considered accumulative and toxic compounds. Their presence as contaminants in aquatic environments may cause serious problems to human beings and other organisms [28]. The migration of pesticides to groundwater and surface water has become an issue of great concern, and numerous incidents of contamination have been documented in developed countries [29]. Organophosphorous pesticides such as methyl parathion and dichlorvos are commonly used in Third-World countries like India where there are poor environmental controls for increasing agricultural productivity and they are detected in various environmental matrices such as soil, water and air because of their widespread use [30,31].

In the present work, we attempted to combine the well-known photocatalytic properties of TiO_2 and the properties of zeolites as TiO_2 supports to synthesize heterogeneous photocatalytic materials. They were prepared by impregnation of titanium (IV) isopropoxide onto three different zeolites (HBETA, HY and HZSM5) and characterized by a series of complementary techniques: X-ray diffraction (XRD), transmittance–Fourier transform infrared spectroscopy (FTIR), and UV–visible diffuse reflectance spectroscopy (DRS). The materials were evaluated in the photodecomposition of organophosphate pesticide dichlorvos. To the best of our knowledge, this is the first time that these materials have been successfully synthesized and tested in the photodegradation of this pollutant.

2. Experimental

2.1. Preparation of photocatalysts

The supports employed were BETA, ZSM5 and Y zeolites. Zeolite HY was provided by Aldrich; the other zeolites were synthesized by means of the hydrothermal crystallization method using tetrapropylammonium hydroxide (TPAOH, Fluka) for the ZSM5 structure [32] and tetraethylammonium hydroxide (TEAOH, Merck) for the BETA structure [33] as directing agents. The ammonium forms of zeolite were prepared by ion exchange of the as-prepared Na-zeolite form with 1 M ammonium chloride solution at 80 °C for 40 h. The HBETA and HZSM5 were obtained by means of a thermal treatment under nitrogen flow for 8 h at 500 °C and then calcinations in air at the same temperature for 10 h. The catalysts supported on zeolitic matrices (HBETA, HY and HZSM5) were prepared by using an appropriate amount of titanium (IV) isopropoxide (Aldrich chemistry, 97%) and zeolite matrix in ethanol (Cicarelli), which was mechanically stirred for 4 h at ambient temperature. Then the solvent was removed by rotary evaporation. In the HBETA matrix, the amount of titanium (IV) isopropoxide was varied with the purpose of generating in situ TiO_2 concentrations of 5, 10, 20, and 30 wt% in the final solid. The mixture was then dried at 110 °C and calcined in air at 450 °C. They were denominated TiO_2/HBETA(5%), TiO_2/HBETA(10%), TiO_2/HBETA(20%) and TiO_2/HBETA(30%). In order to compare the activity, TiO_2/HY(20%) and TiO_2/HZSM5(20%) were prepared with 20 wt% of TiO_2 in the final solid in HY and HZSM5, respectively. P25 standard TiO_2, which was included for comparison with the supported catalyst, was kindly supplied by Degussa.

2.2. Characterization

The powder XRD diffraction patterns of the materials were collected on a PANalytical X'pert PRO diffractometer equipped with Cu Kα (1.54 Å) in the range of 2θ from 5 to 50° (for HBETA and HY) and 5–60° (for HZSM5) in steps of 0.05° with a count time of 2 s at each point. The crystallite size (Dc) of the new crystalline phase was estimated by XRD using the Scherrer equation. BET surface area determinations were carried out with Micromeritics ASAP 2000 equipment. Infrared (IR) studies were performed on a JASCO 5300 FTIR spectrometer. The spectra in the lattice vibration region were performed using KBr 0.05% wafer technique and they were carried out from 1800 to 400 cm^{-1} in 16 consecutive registers of 4 cm^{-1} resolution each. UV–visible diffuse reflectance spectroscopy (DRS) in absorbance mode was recorded using an Optronics OL 750-427 spectrometer in the wavelength range of 200–900 nm.

The Si/Al relation of HBETA and HZSM5 zeolites was determined by atomic absorption in a Perkin Elmer Analyst 800 spectrometer after the digestion of the samples by microwave in a Milestone ETHOS 900 digester. In order to determine the Bronsted/Lewis acid site relation and concentration of acidic sites of the zeolitic matrices, pyridine (Py) adsorption experiments were carried out on self-supporting wafers (8–10 mg/cm^2) using a thermostated cell with CaF_2 windows connected to a vacuum line. Pyridine (3 Torr) was adsorbed at room temperature and desorbed at 400 °C and 10^{-4} Torr for 1 h. The Bronsted/Lewis relation was calculated from the maximum intensity of the adsorption bands at 1545 cm^{-1} and 1450–1460 cm^{-1}, for Bronsted and Lewis sites, respectively, and quantified using the literature data of the integrated molar extinction coefficients [34], which are independent of the catalysts or strength of the sites.

Table 1
Specific surface area, crystallite size and optical band gap of TiO_2, HBETA, HY, HZSM5 and TiO_2/zeolite samples.

Samples	S_{BET} (m^2/g)	Dc (nm)[a]	E_g (eV)[b]
HBETA	585		5.40
TiO_2/HBETA(5%)	522	14.1	3.52
TiO_2/HBETA(10%)	516	15.2	3.20
TiO_2/HBETA(20%)	510	12.9	2.98
TiO_2/HBETA(30%)	466	16.1	2.98
HY	485		5.10
TiO_2/HY(20%)	346	17.5	3.58
HZSM5	355		5.70
TiO_2/HZSM5(20%)	342	16.4	3.47

[a] Dc values of TiO_2/zeolite samples were calculated using $2\theta = 25.4^\circ$ assigned to the (1 0 1) crystal plane.
[b] ±0.05 eV.

2.3. Photocatalytic degradation of dichlorvos

The catalytic activity of the materials was evaluated in the photodegradation of dichlorvos (DDVP Pestanal, Fluka) in water, at 25 °C. The tests were carried out employing a 125 W high-pressure mercury lamp (the maximum emission is 365 nm and the light intensity is about 20 mW/cm^2) placed inside a Pyrex-glass jacket, thermostated by water circulation, and immersed in the DDVP solution contained in a 400 mL cylindrical Pyrex-glass reactor. For comparison purposes, solar light was utilized for the best supported catalyst. The catalyst was maintained in suspension by stirring and air was continuously bubbled. Previously, the DDVP solution (400 mL, 1×10^{-4} mol L^{-1}, 22.1 ppm) containing 100 mg of catalyst was magnetically stirred in the absence of light for 30 min to ensure that the adsorption–desorption equilibrium of DDVP on the surface of the materials was attained. During the course of the experiments, samples were periodically extracted, filtered using a Millipore syringe adapter (porosity, 0.22 μm) and then analyzed. The variation of the pesticide concentration as a function of irradiation time was determined using a Shimadzu double-beam UV-Visible spectrophotometer, measuring the absorbance at 210 nm [35]. The extent of DDVP mineralization was determined using the Total Organic Carbon, Shimadzu 5050. In order to evaluate the possibility of TiO_2 leaching, a reaction was conducted under similar conditions to that of the degradation, only that after 30 min of reaction the catalyst was removed and then, the reaction continued as before up to 240 min.

3. Results and discussion

3.1. Catalyst characterization

The surface area (S_{BET}) of HBETA, HY, HZSM5 and TiO_2/zeolite samples, determined from N_2 adsorption–desorption isotherms using Brunauer–Emmett–Teller (BET) method, is listed in Table 1. In all the cases, the S_{BET} decreases with the increment of TiO_2 content in the sample. This could be due to deposition of TiO_2 particles on the zeolite matrix surface and pore blocking. The greatest decrease was observed for TiO_2/HY zeolite, which has the largest pore size with respect to the other matrices [36], favoring the formation of larger crystals of TiO_2 in the pores, blocking them. This behavior can be checked with the results of XRD (Fig. 1).

In order to confirm the structure and crystallinity of TiO_2/zeolite catalysts, an XRD study was carried out. Fig. 1 shows the XRD patterns of HBETA (a) and different titania-supported catalysts (b–e). The figure shows the characteristic signals of the parent HBETA catalyst at 2θ angles of 7–8° and 21–22° [37,38]. These data were confirmed with JC-PDF file for BETA zeolite. However, its intensity decreases in parallel with the increment of TiO_2 content. TiO_2/HBETA prepared in this study showed a diffraction peak

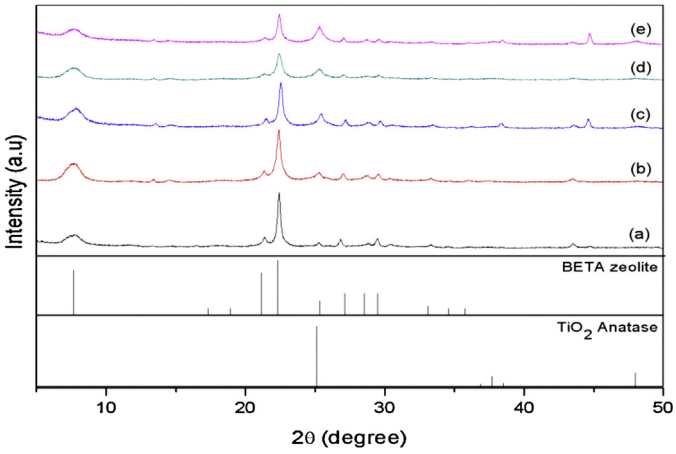

Fig. 1. XRD pattern of (a) HBETA zeolite, (b) TiO_2/HBETA(5%), (c) TiO_2/HBETA(10%), (d) TiO_2/HBETA(20%), and (e) TiO_2/HBETA(30%).

at 25.4°, which was assigned to the characteristic reflection from the (1 0 1) plane of anatase [39]. The peak intensity at $2\theta = 25.4^\circ$ increased with an increasing amount of TiO_2 loaded on zeolite [23,40–43].The peak at 48.5° is barely observed since the amount of TiO_2 would not be enough to give clear diffraction peaks.On the other hand, no peak assigned to the rutile phase ($2\theta = 27.4^\circ$) was observed in the XRD patterns of all TiO_2/HBETA catalysts used in the present study. For most photocatalytic reaction systems, it is generally accepted that the anatase phase has higher activity than rutile, and this enhancement in photoactivity has been ascribed to the higher Fermi level of anatase than that of rutile by about 0.1 eV [39].

The XRD patterns of HY and HZSM5 matrices (see supplementary data, Figure S1) show the characteristic peaks, 2θ angles of 6.3° and 15.92°, and 2θ angles of 7–8° and 21–22°, respectively. TiO_2/HY(20%) and TiO_2/HZSM5(20%) materials, as well as other supported catalysts, show the anatase phase but not the rutile phase. Therefore, it can be suggested that the anatase particles are favorably stabilized on the surface of the zeolite matrix [23]. However, the absence of characteristic peaks assigned to the rutile phase could also be due to the its presence in a lower proportion than the anatase phase or in a high dispersion degree (very small crystals undetected by XRD). In TiO_2/HY(20%), some peaks of the starting matrix disappeared and the baseline was modified, resulting in a less crystalline catalyst compared with the other supported catalysts. Zeolite Y is more sensible than other zeolites during the incorporation of other substances in the matrix. This is partly due to the instability of zeolites Y at low Si/Al ratios (see supplementary data T1) [44,45].

The crystallite size (D_C) of the new crystalline phase, estimated by XRD using the Scherrer equation, seems to be independent of the TiO_2 content in the prepared materials in the majority of the cases. In general, an increase in the TiO_2 content causes an increase in the crystal size, but in the case of TiO_2/HBETA(20%) the crystallite size is smaller, which maybe because this amount of TiO_2 is appropriate to generate smaller crystals of TiO_2 and achieve good dispersion (Table 1). Also, the available surface area is large enough to accommodate new crystals instead of generating larger crystals.

The FTIR spectrum of HBETA (Fig. 2a) shows the bending mode of water at 1640 cm^{-1}. The framework asymmetric vibrations of Si–O–Si and Si–O–Al give an intense broad band between 1300 and 850 cm^{-1}, and the symmetric vibration at 800 cm^{-1}. The spectra b–e shown in the same figure correspond to 5, 10, 20 and 30 wt% TiO_2/HBETA catalysts. Though the spectra appear similar, there are still some variations in the region of the bending modes of HBETA framework. The symmetric vibration of Si–O–Si

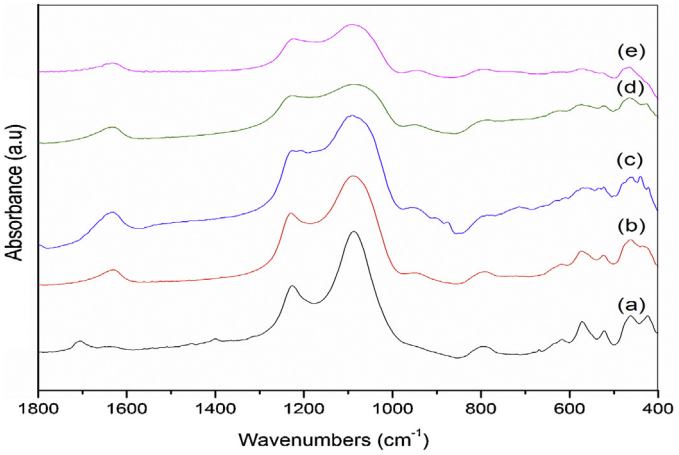

Fig. 2. FTIR of (a) HBETA zeolite, (b) TiO_2/HBETA(5%), (c) TiO_2/HBETA(10%), (d) TiO_2/HBETA(20%), and (e) TiO_2/HBETA(30%).

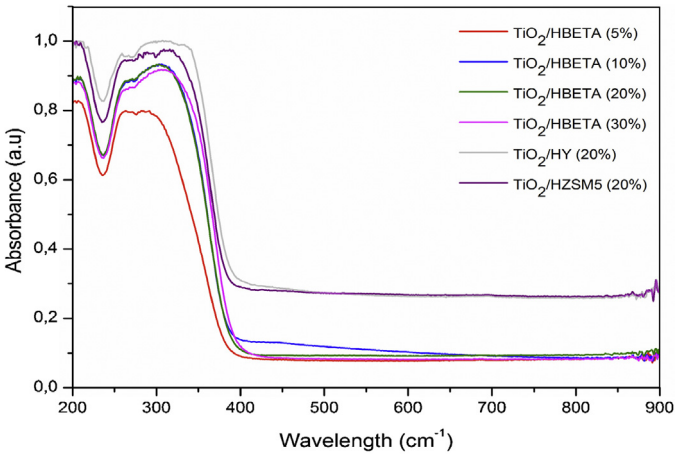

Fig. 3. DRS of the catalyst supported on the different zeolitic matrices with TiO_2.

(800 cm^{-1}) is clearly resolved in the spectrum of HBETA (spectrum a) but its intensity decreases with the increase in TiO_2 loading. This is attributed to intense Ti–O stretching overlapped with Si–O–Si vibration, due to calcination of the samples at 450 °C [42,46]. The other bands also show a decrease in intensity, which can be due to a dilution effect by the increase in TiO_2 loading and a decrease in the zeolite matrix loading.

The intensity of the O–H_2 bending mode at 1640 cm^{-1} increases up to 10 wt%, but decreases for 20 and 30 wt% TiO_2/HBETA. There may be a transfer of outer surface Bronsted acid sites of HBETA to TiO_2 particles up to 10 wt% TiO_2 loading. Hence, both negatively charged Si–O–Al bridge and protonated TiO_2 particles could adsorb water. But the excess TiO_2 particles block the acid sites in 20 and 30 wt% TiO_2/HBETA [42]. Hence, the intensity of the OH_2 bending mode decreases for higher loading of TiO_2/HBETA.

For the other matrices, the FTIR spectra in the range 1800–400 cm^{-1} (see supplementary data, Figure S2) present vibrations assigned to the internal bonds of a TO_4 tetrahedral structure (T = Si or Al) that are insensitive to changes in the zeolite structure, asymmetrical stretching (1300–900), symmetrical stretching (850–750 cm^{-1}) and to (O–T–O) deformation (600–400 cm^{-1}).

In all the cases, no band in the region near 960 cm^{-1} was detected, which could be assigned to the antisymmetric stretching vibration of the Ti–O–Si bonds [43,46,47]. Therefore, the tetrahedral Si sites were not replaced with Ti during preparation. So, we can conclude that TiO_2 was deposited on the zeolite surface [23].

The diffuse reflectance spectrum of zeolitic matrices (see supplementary data, Figure S3) presents two bands at 216 and 300 nm assigned to the first one that arose from the Al–O charge-transfer transition of four-coordinated framework aluminum, the second one being attributed to structures with highly ordered octahedral symmetry [48,49]. The UV–vis diffused reflectance spectra of TiO_2/HBETA, TiO_2/HY(20%) and TiO_2/HZSM5(20%) samples are shown in Fig. 3. In the supported catalyst, the absorption band at 200–250 nm is due to electron transfer from the ligand oxygen to an unoccupied orbital of the Ti^{4+} framework [50]. The spectra are also characterized by an intense band centered at 320 nm, corresponding to charge transfer from the valence band (O 2p) to the conduction band (Ti 3d) [51]. According to the literature, a band around 320 nm might be due to the presence of anatase in the extra framework [52]. The UV–vis DRS results may confirm the absence of a Ti–O–Si linkage in these systems [25].

The band gap energy values (E_g), estimated from UV–Vis–DRS spectra using Kubelka–Munk remission function [53], are listed in Table 1. The E_g values of zeolitic matrices (HBETA, HY and HZSM5) without TiO_2 and TiO_2/zeolites are similar to those reported in the literature [54,55]. The E_g values decrease slightly with the increment of the TiO_2 content for the HBETA zeolite up to 20% TiO_2 loading, and then the E_g values remain practically unchanged no matter the TiO_2 content in the samples. For the different zeolitic matrices with the same loading, the values indicate that there are differences in the band gap for the TiO_2/HY(20%) sample, whose value was relatively high (3.58 eV). This result may be due to the low crystallinity in this sample compared with other matrices. The higher number of imperfections and defects in the TiO_2 structure may act as recombination centers for the electron/hole pairs, which in turn will result in poor efficiency in photocatalysis [43].

3.2. Photocatalytic activities

Prior to photocatalytic experiments, the DDVP solution (400 mL, 1×10^{-4} mol L^{-1}, 22.1 ppm) with 100 mg of catalyst was magnetically stirred in the absence of light to study the adsorption on the surface of the materials. The pesticide adsorption over the zeolitic matrices follow a Langmuir isotherm behavior. From the linealized Langmuir isotherm the maximum adsorbed amounts were obtained. These values were 0.02, 0.01 and 0.006 mg of DDVP for mg catalyst for HBETA, HY and HZSM5, respectively. These behaviors of the zeolitic matrices agree with the structural properties and stability of each material. The results revealed the greater adsorption of DDVP on HBETA and hence, it was chosen as the suitable support for further studies. The lower adsorption property of HY and HZSM5 compared to HBETA is attributed to the higher hydrophilic nature of HY and lower surface area of HZSM5. Apart from these facts, the larger number of acid sites in HBETA (see supplementary data, Table S1) could also be yet another reason for the better adsorption of DDVP [56]. The DDVP molecule can be efficiently adsorbed on the acid sites of HBETA due to its small size. The maximum adsorption was reached within 30 min, that is, at least 30 min was necessary to ensure that the adsorption–desorption equilibrium of DDVP on the surface of the materials was attained.

The results of the photolysis experiments carried out without any catalyst showed that only 2–5% degradation occurred. In the presence of H-zeolites as catalyst, no significant mineralization was observed, confirming that zeolitic matrices are not in themselves active in the degradation of DDVP.

The effect of TiO_2 percentage in the zeolitic matrices on the photocatalytic activity of DDVP is shown in Table 2. The studies were done using 100 mg of catalyst in 400 mL of DDVP aqueous solution. The degradation percentage was calculated as $X = (C_0 - C/C_0) \times 100$, where C_0 is the original DDVP concentration and C the remaining DDVP concentration in solution at specific time intervals. It is

Table 2
Degradation percentages for DDVP at 240 min, reaction rate (k_r), adsorption equilibrium constant (K_{ads}) and TOC values. The experimental conditions were air; pH 5; [DDVP] = 1×10^{-4} mol L^{-1}; [catalyst] = 250 mg/L; UV lamp.

Catalyst	Degradation percentage (%)	k_r (mol L^{-1} min^{-1})	K_{ads} (mol^{-1} L)	TOC (ppm)
TiO_2	90.04 (±0.02)	2.52×10^{-6}	3.28×10^{3}	3.47
HBETA	30.02 (±0.03)	3.33×10^{-7}	3.88×10^{3}	4.82
TiO_2/HBETA(5%)	67.28 (±0.05)	1.10×10^{-6}	2.67×10^{3}	3.45
TiO_2/HBETA(10%)	77.35 (±0.06)	2.32×10^{-6}	2.91×10^{3}	2.96
TiO_2/HBETA(20%)	89.96 (±0.05)	2.94×10^{-6}	3.27×10^{3}	2.75
TiO_2/HBETA(30%)	75.34 (±0.04)	1.89×10^{-6}	2.03×10^{3}	2.98
HY	22.82 (±0.04)	3.33×10^{-7}	3.42×10^{3}	4.84
TiO_2/HY(20%)	47.54 (±0.03)	5×10^{-7}	2.04×10^{3}	4.13
HZSM5	18.66 (±0.07)	3.33×10^{-7}	3.03×10^{3}	4.82
TiO_2/HZSM5(20%)	71.40 (±0.05)	5×10^{-7}	2.89×10^{3}	3.32

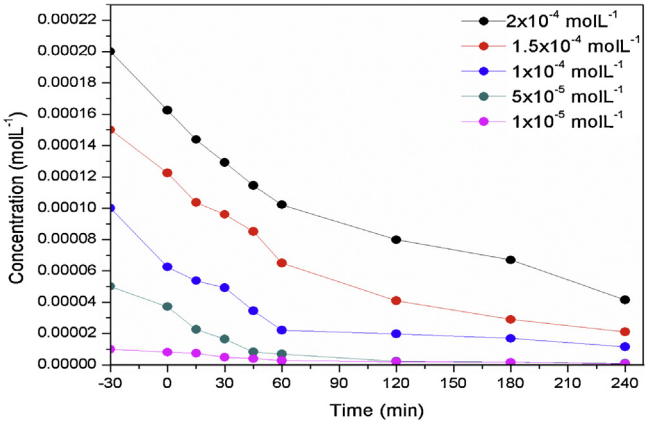

Fig. 4. DDVP photocatalityc degradation at different initial concentration with TiO_2/HBETA (20%).

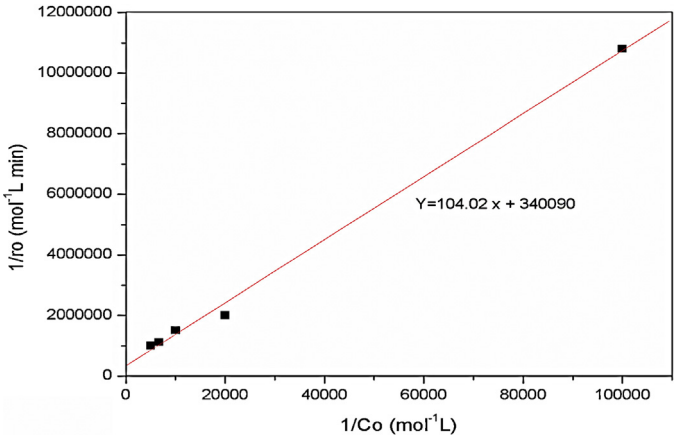

Fig. 5. Linearization of Langmuir–Hinshelwood equation.

known that the photocatalytic reaction rate of most organic compounds is described by pseudo-first-order kinetics that is rationalized in terms of the Langmuir–Hinshelwood model, modified to accommodate reactions occurring at a solid–liquid interface [57]:

$$r_o = -\frac{dc}{dt} = \frac{k_r K C_o}{1 + K C_o} \quad (1)$$

where r_o is the initial rate of DDVP degradation, C_o its initial concentration, K the equilibrium constant and k_r the degradation rate at maximum coverage for the experimental conditions [58]. Equation (1) is linearized by its reciprocal expression (2):

$$\frac{1}{r_o} = \frac{1}{k_r} + \frac{1}{k_r K C_o} \quad (2)$$

For this purpose, experiments at five different initial concentrations of DDVP (Fig. 4) with TiO_2/HBETA(20%) were carried out. The conditions were the same as those for photocatalytic reactions, 400 mL of DDVP solution with 100 mg of catalyst. The r_o values were independently obtained from these curves by the linear fit, using only the experimental points during the first minutes of illumination.

With our experimental data, Fig. 5 was plotted with Equation (2). From the intersection of this straight line with the ordinate $1/k_r$ results and hence, the value of the reaction rate is $k_r = 2.94 \times 10^{-6}$ mol L^{-1} min^{-1}. From the slope of this line, the equilibrium constant, $K = 3.27 \times 10^{3}$ mol^{-1} L, was calculated.

The same procedure was performed for each of the catalysts. The results are listed in Table 2.

The extent of DDVP mineralization was measured at the end of reaction by TOC and the results are listed in Table 2. The initial TOC of DDVP was 4.86 ppm.

For the catalysts supported on the zeolitic matrix HBETA, the increment of TiO_2 content in TiO_2/HBETA samples from 5 to 20 wt% produces a continuous increment of the photocatalytic activity at 240 min. The decline in the degradation of samples with loadings higher than TiO_2/HBETA(20%) could be due to the presence of TiO_2 particle aggregates of greater size on the zeolite matrix surface. As shown in Table 1 and by XRD, the crystallite size is larger in TiO_2/HBETA(30%) than in TiO_2/HBETA(20%). Moreover, at higher percentage loading, the excited particles may not be close to the zeolite surface and hence, its conduction band electron is not delocalized over zeolite. As a result, there could be much electron–hole recombination giving a low degradation rate. Additionally, the increment of the catalytic activity can also be due to the lower band gap values of the samples with higher TiO_2 contents, which would increase the absorption capacity of higher wavelength radiation.

The differences in the behaviors of the zeolitic matrices in the photocatalytic activity of DDVP can be associated with the structural properties and stability of each material. The lower activity for zeolite ZSM5 could be associated with its microporous structure (pores defined by ten member rings) that hinders the access of large molecules to the internal acid sites. In addition and in comparison with the other matrices, it has lower surface area and a fewer number of acid sites. The lower adsorption property and photocatalytic activity of HY compared to HBETA is attributed to the higher hydrophilic nature of HY, which allows water to pass through its channels but it does not allow the passage of organic molecules such as those of DDVP. Also, as aforementioned, zeolite Y is more sensible and unstable than other zeolites due to low Si/Al ratios. The loss of crystallinity because of the incorporation of TiO_2 and the thermal treatment reduce the activity of the catalytic material. In these studies BETA zeolite presents better results due to its three-dimensional pore system with straight channels of 0.73 nm × 0.65 nm and tortuous channels of 0.55 nm × 0.55 nm with 1.0 nm channel intersections, with higher accessibility to its

active sites (pores defined by twelve member rings), which makes it more active.

The rate of degradation is related to the formation of OH• radical, which is the critical species in the degradation process [59]. The equilibrium adsorption of reactants on the catalyst surface and the reaction rate of OH• radicals with other chemicals are also significant in the rate of degradation [60]. The hydroxyl radicals are formed through the reaction of holes with adsorbed OH^- and H_2O on the TiO_2 surface. The oxidizing power of the OH• radicals is strong enough to oxidize adsorbed DDVP on the surface of TiO_2/zeolites.

After 240 min of irradiation, the amount of degraded DDVP was close to 90% with TiO_2/HBETA(20%), but the mineralization degree was close to 44%. The TOC values decreased with the increase in the degradation percentage, but were slightly lower than the amount of degraded DDVP as a result of the formation of organic intermediates. These results are in agreement with previous reports that indicate the formation of phosphate-containing intermediates [23,58]. The *O,O,O*-trimethyl phosphoric ester and *O,O*-dimethyl phosphonic ester have been reported as the main intermediates during the photodegradation of DDVP [61]. These by-products appear to be less toxic than the parent compound, so a less contaminant solution than the starting solution is obtained. The complete degradation and mineralization of the pollutant was obtained under these conditions in 360 and 540 min of reaction with TiO_2/HBETA(20%), respectively. We assume that once all the DDVP have been degraded, the phosphate intermediates start to be degraded.Additionally, comparative studies were performed to understand the role of the support during the photocatalytic degradation between TiO_2/HBETA(20%) and bulk TiO_2 (Degussa P25). The reaction was carried out with 20 mg of TiO_2 P25 and 400 mL of DDVP solution 1×10^{-4} mol L^{-1}, which is equivalent to 20% in the matrix. In Table 2, at 240 min of reaction, it can be seen that the TiO_2-supported system shows similar degradation to that of bulk TiO_2, both materials reaching almost the same degradation. This may suggest that the zeolite matrix does not affect the degradation capacity and the photocatalytic properties of TiO_2. But supported TiO_2 is easier to separate than the commercial one, so it can be easily reused. Also, the dispersion of TiO_2 over zeolite material avoids particle–particle aggregation and light scattering by TiO_2 [23]. TOC results revealed that pure TiO_2 required more time for the complete mineralization of DDVP.

The experiment with solar light was performed with TiO_2/HBETA(20%), the degradation percentage achieved was 58% at 240 min of reaction. Kinetic and adsorption equilibrium constants were calculated as: k_r: 2.31×10^{-6} mol L^{-1} min^{-1} and K: 2.86×10^3 mol^{-1} L, respectively. This result is mainly due to the different initial photon flow of both light sources [57]. With an improvement in the photocatalytic system, making solar rays focus on the photoreactor, the system applied may be better.

3.3. Reusability of the catalysts

To evaluate the reusability of the catalysts we chose TiO_2/HBETA(20%) because it was the catalyst with better performance in this study. At the end of the first photocatalytic cycle, the catalyst was separated from the resulting suspension by filtering, washed, oven dried at 70 °C, and then reused without any calcination treatment. The same procedure was employed after the second and all the cycles of use. The percentage of degraded DDVP after each cycle of use, together with the mineralization degree, is shown in Fig. 6.

The comparison of the DDVP degradation degree reached at the end of the first cycle showed that the degradation rate decreased slightly and then kept constant. The decrease in the degradation percentage was probably due to the accumulation of organic

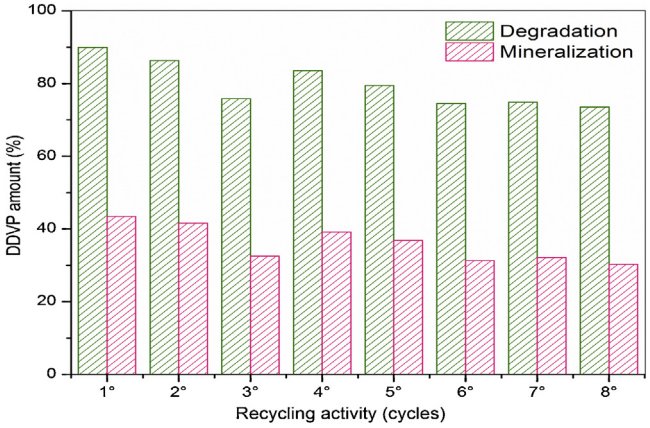

Fig. 6. DDVP degradation and mineralization degree as a function of the number of cycles of use for TiO_2/HBETA(20%).

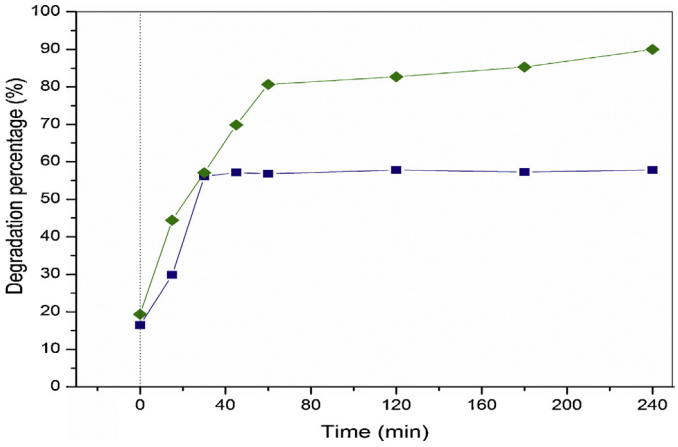

Fig. 7. Evolution of DDVP after photocatalysis with TiO_2/HBETA(20%) (♦) and leaching test (■) with the same catalyst filtrate at the 30 min.

intermediates in the cavities and on the surface of the catalyst affecting the adsorption of DDVP, and reducing the activity of the catalytic material. Finally, these results show that these materials can be reused without noticeable activity loss during at least eight cycles, and the synthesized materials can be considered as suitable photocatalysts to degrade organophosphorous pesticides.

3.4. Titanium dioxide leaching

It is worth noting that no leaching of titanium dioxide from TiO_2/zeolite samples occurs during the reaction. TiO_2 could not be detected in the liquid filtrate after each cycle of use. Additionally, no significant conversion of DDVP was observed when we evaluated the possibility of TiO_2 leaching. This reaction was carried out under similar conditions to that of the degradation, except that after 30 min of reaction the catalyst was removed. As can be seen in Fig. 7, the reaction stopped. These observations strongly suggest that the reaction proceeds heterogeneously over the catalyst.

4. Conclusions

Materials based on TiO_2 supported on zeolitic matrices (HBETA, HY and HZSM5) were synthesized by the in situ generation of TiO_2 using titanium (IV) isopropoxide and ethanol. XRD patterns indicate that all materials presented crystalline phases and only showed the presence of the anatase phase. In FTIR no band in the region near 960 cm^{-1} was detected, so it can be concluded that TiO_2

was deposited on the surface of zeolites. In the TiO_2/HBETA samples, S_{BET} decreased with the increase of the TiO_2 content as a result of zeolite pore blocking, attributed to clogging of zeolite pores by TiO_2 species. Comparing the different matrices with the same TiO_2 content, TiO_2/HBETA(20%) shows the highest surface area.

The results of the present investigation indicate that the most convenient catalyst for photocatalytic degradation is TiO_2/HBETA(20%). At higher TiO_2 content the degradation percentage is lower, which could be due to the presence of TiO_2 particle aggregates of greater size on the zeolite matrix surface. This is evidenced by the crystal size calculated by XRD.

TiO_2/HBETA(20%) presented more activity than TiO_2/HY(20%) and TiO_2/HZSM5(20%) due to higher adsorption of DDVP on it. It has more surface area and a lower band gap value too, which makes it more effective. The complete degradation and mineralization of the pollutant was obtained in 360 and 540 min of reaction, respectively. These materials can be reused without noticeable activity loss during at least eight cycles. The mineralization degree is lower than the degradation percentage due to the formation of organophosphorous intermediates that are less toxic than the starting material.

According to the results presented in this work, the materials obtained by in situ generation of TiO_2 onto zeolitic matrices, HBETA, HY and HZSM5, present suitable properties to be used as catalysts in the photocatalytic treatment of wastewater that contains DDVP insecticide. The TiO_2/HBETA(20%) catalysts prepared in this study yielded degradation percentages closer to commercial TiO_2 P25. The advantage of supported catalysts, in comparison with the commercial ones, is mainly their easy separation and reuse.

Acknowledgements

This project was partially supported by: Mincyt-Córdoba PID 000121 and PID UTN 25/E172. We thank CONICET: L.B.Pierella, L.R. Pizzio, M. S. Renzini, C. Leal Marchena and S. Gomez.

Appendix A. Supplementary data

Supplementary data associated with this article can be found, in the online version, at http://dx.doi.org/10.1016/j.apcatb.2014.06.047.

References

[1] M.N. Chong, B. Jin, C.W.K. Chow, C. Saint, Water Res. 44 (2010) 2997–3027.
[2] N. Daneshvar, D. Salari, A.R. Khataee, J. Photoch. Photobio. A: Chem. 157 (2003) 111–116.
[3] M.L. Satuf, R.J. Brandi, A.E. Cassano, O.M. Alfano, Ind. Eng. Chem. Res. 44 (2005) 6643–6649.
[4] J-M. Herrmann, Catal. Today 53 (1999) 115–129.
[5] P.R. Gogate, A.B. Pandit, Adv. Environ. Res. 8 (2004) 501–551.
[6] M. Pratap Reddy, A. Venugopal, M. Subrahmanyam, Appl. Catal. B: Environ. 69 (2006) 164–170.
[7] V. Durga Kumari, M. Subrahmanyam, K.V. Subba Rao, A. Ratnamala, M. Noorjahan, K. Tanaka, Appl. Catal. A: Gen. 234 (2002) 155–165.
[8] V. Fuchs, L. Méndez, M. Blanco, L. Pizzio, Appl. Catal. A: Gen. 358 (2009) 73–78.
[9] C. Wang, H. Shi, Y. Li, Appl. Surf. Sci. 257 (2011) 6873–6877.
[10] Y. Xu, C.H. Langford, J. Phys. Chem. B 101 (1997) 3115–3121.
[11] A. Bhattacharyya, S. Kawi, M.B. Ray, Catal. Today 98 (2004) 431–439.
[12] M.V. Phanikrishna Sharma, V. Durga Kumari, M. Subrahmanyam, Chemosphere 73 (2008) 1562–1569.
[13] C. Anderson, A.J. Bard, J. Phys. Chem. 99 (1995) 9882–9885.
[14] G.P. Lepore, L. Persaud, C.H. Langford, J. Photochem. Photobiol. A: Chem. 98 (1996) 103–111.
[15] Y. Xu, W. Zheng, W. Liu, J. Photochem. Photobiol. A: Chem. 122 (1999) 57–60.
[16] C. Minero, F. Catozzo, E. Pelizzetti, Langmuir 8 (1992) 481–486.
[17] C. Anderson, A.J. Bard, J. Phys. Chem. B 101 (1997) 2611–2616.
[18] T. Torimoto, Y. Okawa, N. Takeda, H. Yoneyama, J. Photochem. Photobiol. A: Chem. 103 (1997) 153–157.
[19] J. Hermann, J. Matos, J. Disdier, C. Guillard, J. Laine, S. Malato, J. Blanco, Catal. Today 54 (1999) 255–265.
[20] H. Yoneyama, T. Torimoto, Catal. Today 58 (2000) 133–140.
[21] Y. Xu, C.H. Langford, J. Phys. Chem. 99 (1995) 11501–11507.
[22] N. Takeda, M. Ohtani, T. Torimoto, S. Kuwabata, H. Yoneyama, J. Phys. Chem. 101 (1997) 2644–2649.
[23] S. Gomez, C. Leal Marchena, L. Pizzio, L. Pierella, J. Hazard. Mater. 258–259 (2013) 19–26.
[24] M.V. Shankar, S. Anandan, N. Venkatachalam, B. Arabindoo, V. Murugesan, Chemosphere 63 (2006) 1014–1021.
[25] M.V. Phanikrishna Sharma, V. Durgakumari, M. Subrahmanyam, J. Hazard. Mater. 160 (2008) 568–575.
[26] P.K. Dutta, Y. Kim, Curr. Opin Solid State Mater. Sci. 7 (2003) 483–490.
[27] M.V. Phanikrishna Sharma, K. Lalitha, V. Durgakumari, M. Subrahmanyam, Sol. Ener. Mat. Sol. C 92 (2008) 332–342.
[28] S.A. Naman, Z.A.-A. Khammas, F.M. Hussein, J. Photochem. Photobiol. A: Chem. 153 (2002) 229–236.
[29] J. Senthilnathan, Ligy Philip, Chem. Eng. J. 172 (2011) 678–688.
[30] S.K. Golfinopoulos, A.D. Nikolaou, M.N. Kostopoulou, N.K. Xilourgidis, M.C. Vagi, D.T. Lekkas, Chemosphere 50 (2003) 507–516.
[31] J. Senthilnathan, L. Philip, J. Environ. Sci. Health B 44 (2009) 262–270.
[32] P. Chu, Crystalline zeolite ZSM-11, US Patent No. 3,709,979 (1972).
[33] S. Valencia, M.A. Camblor Fernandez, A. Corma, J. Perez Pariente, Síntesis de zeolita Beta, U.S. Patent 2,124,142 (1999).
[34] C.A. Emeis, J. Catal. 141 (1993) 347–354.
[35] M. Atiqur Rahman, M. Muneer, Desalination 181 (2005) 161–172.
[36] J. Jae, G.A. Tompsett, A.J. Foster, K.D. Hammond, S.M. Auerbach, R.F. Lobo, G.W. Huber, J. Catal. 279 (2011) 257–268.
[37] M.S. Renzini, U. Sedrán, L.B. Pierella, J. Anal. Appl. Pyrolysis 86 (2009) 215–220.
[38] K.K. Cheralathan, I. Sudarsan Kumar, M. Palanichamy, V. Murugesan, Appl. Catal. A: Gen. 241 (2003) 247–260.
[39] K. Porkodi, S. Daisy Arokiamary, Mater. Charact. 58 (2007) 495–503.
[40] S. Yamaguchi, T. Fukura, Y. Imai, H. Yamaura, H. Yahiro, Electrochim. Acta 55 (2009) 7745–7750.
[41] H. Chen, A. Matsumoto, N. Nishimiya, K. Tsutsumi, Colloid. Surf. A 157 (1999) 295–305.
[42] M. Mahalakshmi, S. Vishnu Priya, B. Arabindoo, M. Palanichamy, V. Murugesan, J. Hazard. Mater. 161 (2009) 336–343.
[43] D.I. Petkowicz, R. Brambilla, C. Radtke, C. Silva da Silva, Z.N. da Rocha, S.B.C. Pergher, J.H.Z. dos Santos, Appl. Catal. A: Gen. 357 (2009) 125–134.
[44] S. Koichi, N. Yoichi, M. Nobuyuki, I. Motoyasu, S. Hiromichi, Microporous Mater. 59 (2003) 133–146.
[45] F. Azzolina Jury, I. Polaert, L. Estel, L.B. Pierella, Appl. Catal. A Gen. 453 (2013) 92–101.
[46] C. Wang, C. Lee, M. Lyu, L Dyes Pigm. 76 (2008) 817–824.
[47] Y. Kim, M. Yoon, J. Mol. Catal. A: Chem. 168 (2001) 257–263.
[48] E.D. Garbowski, C. Mirodatos, J. Phys. Chem. 86 (1982) 97–102.
[49] M.A. Zanjanchi, A. Razavi, Spectrochim. Acta A 57 (2001) 119.
[50] D.I. Petkowicz, S.B.C. Pergher, C.D. Silva da Silva, Z.N. da Rocha, J.H.Z. dos Santos, Chem. Eng. J. 158 (2010) 505–512.
[51] J. Liqiang, S. Xiaojun, C. Weimin, X. Zili, D. Yaoguo, F. Honggang, J. Phys. Chem. Solids 64 (2003) 615–623.
[52] F. Geobaldo, S. Bordiga, A. Zecchina, E. Giamello, G. Leofanti, G. Petrini, Catal. Lett. 16 (1992) 109–115.
[53] S.P. Tandon, J.P. Gupta, Phys. Stat. Solidi 38 (1970) 363–367.
[54] E. Joselevich, I. Willner, J. Phys. Chem. 98 (1994) 7628–7635.
[55] G. Yan, J. Long, X. Wang, Z. Li, X. Fu, CR Chim. 11 (2008) 114–119.
[56] K.V. Subba Rao, M. Subrahmanyam, Photochem. Photobiol. Sci. 1 (2002) 597–599.
[57] P. Oancea, T. Oncescu, J. Photochem. Photobiol. A: Chem. 199 (2008) 8–13.
[58] E. Evgenidou, K. Fytianos, I. Poulios, Appl. Catal. B: Environ. 59 (2005) 81–89.
[59] M.V. Shankar, B. Neppolian, S. Sakthivel, M. Banumathi Arabindoo, V. Palanichamy, Murugesan, Ind. J. Eng. Mater. Sci 8 (2001) 104–109.
[60] C. Kormann, D.W. Bahnemann, M.R. Hoffmann, Environ. Sci. Technol. 25 (1991) 494–500.
[61] E. Evgenidou, I. Konstantinou, K. Fytianos, T. Albanis, J. Hazard, Mater. B137 (2006) 1056–1064.